Ductility Loss Modelling for BCC Single Crystals

Jean-Paul Lorrain — Tarak Ben-Zineb
Farid Abed-Meraim — Marcel Berveiller

Laboratoire de Physique et Mécanique des Matériaux
ENSAM de Metz, UMR CNRS 7554
4 rue augustin fresnel
F-57078 Metz cedex 3

Jean-Paul.Lorrain@Metz.Ensam.Fr

ABSTRACT. *An elastic-plastic micromechanical behavior model written in the finite strains framework is presented. It is shown that the present model is able to reproduce the behavior for BCC materials during simple and complex loading paths. A ductility criterion based on the ellipticity loss of the elastic-plastic tangent modulus is introduced. Qualitative results obtained with this criterion are in good agreement with expected and literature ones.*

KEYWORDS: *Single Crystal, Ductility, Finite Strains, Crystal Plasticity.*

IJFP – 8/2005. Metal Forming Simulation, pages 135 to 158

1. Introduction

Industrial applications obtained from flat products by forming processes are widely used in many fields from automotive until aeronautics or space without forgetting electrical goods or packaging. Before making the realization of an application by forming, it is necessary to know the ductility limit of the used material. Experimental forming limit diagrams now quantify this limit. But the test protocols associated are far from making unanimity on their real representativeness, and have a high cost in terms of time and money. An idea consists in having a simulation tool able to construct forming limit diagrams numerically.

Much progress have been made in this way for the description of the elastic-plastic material behavior (Asaro, 1983; Asaro *et al.*, 1977; Peirce, 1983, Peirce *et al.*, 1983; Iwakuma *et al.*, 1983). Constitutive laws have been developed at the macroscopic level by using scale transition model like the self-consistent approach (Berveiller *et al.*, 1979), Kröner (1977) or Mori-Tanaka (1973) ones.

Further progress need to be made in order to reach the numerical simulation of forming limit diagrams. The elastic-plastic single crystal behavior have to be better described by integrating the following points:

– effect of creation and annihilation of dislocations on single crystal hardening during complex loading path (which occurs frequently in forming processes),

– effect of the terms linked to single crystal internal stresses and not taken into account in the small strains framework,

– improve active slip systems determination which costs the most in terms of calculus time (a combinatory analysis is needed).

Thus, it is necessary to have a ductility criterion representative of reality. Nowadays many workers are studying the ellipticity loss of the elastic-plastic operator (Petryk, 2000; Rice, 1976) which can be used as a criterion of the material ductility limit.

In this paper a contribution of the modelling of numerical forming limit diagrams is presented. An elastic-plastic behavior model written in the finite strain framework is proposed. It includes the description of the effects of creation and annihilation of dislocations on hardening. A new active slip system determination allowing a considerable gain of computing time is proposed. Numerical results of this model are compared with experiments extracted from literature for different loading paths. Lastly, the criterion introduced by Rice in 1976 is applied to predict ductility loss. Qualitative results are given and compared to literature ones.

2. Single crystal modelling

Single crystal behavior is assumed to be elastic-plastic (time independent) and plastic strain only due to slip on crystallographic planes. Other modes of

deformation like twinning or phase transformation are not taken into account. In the case of BCC materials, slip systems families are: {1 1 1}<1 1 0>, {1 1 1} <1 1 2>. There are 24 slip systems. In order to present the single crystal model studied here: slip systems, kinematics and the hardening would be defined. By combining all those relations the tangent modulus expression would be deduced. If not specified, Einstein's convention is used.

2.1. *Definition of a slip system*

A slip system is defined by a slip direction $\vec{m}$ and a normal to the slip plane $\vec{n}$. The slip amplitude is noted γ. Crystallographic orientation of the single crystal from the crystal frame is needed. Two tensors for each slip system called Schmid's tensors can be introduced:

$$R_{ij}^{g} = \frac{1}{2}\left(m_i n_j + m_j n_i\right)^{g}$$
$$S_{ij}^{g} = \frac{1}{2}\left(m_i n_j - m_j n_i\right)^{g} \qquad [1]$$

R^g is the orientation tensor which allows to pass from the crystal frame to the slip system g. S^g is an skew tensor used in the calculus of lattice rotation.

2.2. *Strain decomposition*

The velocity gradient g can be decomposed into a symmetric part d and a skew one w as:

$$g = d + w \qquad [2]$$

The tensor w corresponds to the rate of lattice total rotation and d corresponds to the rate of total lattice strain. w and d can also be cut into a plastic and an elastic part corresponding to lattice ones as:

$$d = d^{e} + d^{p}$$
$$w = w^{e} + w^{p} \qquad [3]$$

With:

$$d_{ij}^{p} = R_{ij}^{g}\dot{\gamma}^{g}$$
$$w_{ij}^{p} = S_{ij}^{g}\dot{\gamma}^{g} \qquad [4]$$

Where $\dot{\gamma}^g$ is the slip rate over the slip system g.

2.3. *Active slip systems determination*

For a system, the value of the resolved shear stress and its evolution can be defined as:

$$\begin{aligned} \tau^g_{res} &= \sigma_{ij} R^g_{ij} \\ \dot{\tau}^g_{res} &= \hat{\sigma}_{ij} R^g_{ij} \end{aligned} \quad [5]$$

τ^g_{res} is the resolved shear stress on the slip system g, $\hat{\sigma}$ is the corotationnal derivative used for objective derivation.

$$\hat{\sigma}_{ij} = \dot{\sigma}_{ij} - w^e_{ik}\sigma_{kj} - w^e_{jk}\sigma_{ki} \quad [6]$$

A slip system is active if the value of the resolved shear stress reaches a critical value noted τ^g_c, and if his increment reaches the value of the critical resolved shear stress $\dot{\tau}^g_c$ one. It will create a non-zero slip rate on this system. This can be written on the form:

$$\tau^g_{res} < \tau^g_c \Rightarrow \dot{\gamma}^g = 0 \quad [7a]$$

$$\tau^g_{res} = \tau^g_c \text{ and } \dot{\tau}^g_{res} < \dot{\tau}^g_c \Rightarrow \dot{\gamma}^g = 0 \quad [7b]$$

$$\tau^g_{res} = \tau^g_c \text{ and } \dot{\tau}^g_{res} = \dot{\tau}^g_c \Rightarrow \dot{\gamma}^g > 0 \quad [7c]$$

It is important to note that the critical resolved shear stress is different for each slip system. Classical method to choose the set of slip systems which are really active use the minimization of an energy (Franciosi *et al.*, 1991; Busso *et al.*, 2002). In the proposed model a new criterion inspired from viscoplasticity to determine active slip systems is introduced (Ben Zineb *et al.*, 2001; Lorrain *et al.*, 2002). The relations [7a], [7b] and [7c] are put into the form (no summation over the indices):

$$\dot{\gamma}^g = k^g \dot{\tau}^g_c \quad [8]$$

This new formulation allows reducing computing time by a ratio 20 to 1instead of a classical approach. The hardening parameter k^g is defined by (no summation over the indices):

$$k^g = \frac{1}{8H^{gg}}\left(1+\tanh\left(k_0\tau^g_{res}\right)\right)\left(1+\tanh\left(k_1\left(\frac{\tau^g_{res}}{\tau^g_c}-1\right)\right)\right)\left(1+\tanh\left(k_2\dot{\tau}^g_{res}\right)\right) \quad [9]$$

Where H^{gg} is the self-hardening parameter defined in the following (Franciosi, 1984). The relation [9] shows that the hardening parameter is composed of 3 terms; its value would be $1/H^{gg}$ if the conditions [7c] is verified and null in all other cases. Parameters k_0, k_1, k_2 are numerical parameters which are used to have functions with the maximum gradient at 0 (in order to represent a threshold). Values taken by the authors, after making a numerical analysis of their respective influence, are 1 for k_0, k_2 and 20 for k_1.

2.4. *Slip systems rate*

In the case where the slip system g is active (without summation over g):

$$k^g \hat{\sigma}_{ij} R^g_{ij} = \dot{\gamma}^g \quad [10]$$

In the large strain framework the elasticity law takes a form rather different than in the small strains framework (Sidoroff, 1982):

$$\hat{\sigma}_{ij} = \mathrm{C}_{ijkl} d^e_{kl} - \sigma_{ij} d^e_{kk} \quad [11]$$

Where C is the elastic moduli tensor assumed isotropic. The product of [11] by $k^h R^h$ noted R'^h is:

$$R'^h_{ij}\hat{\sigma}_{ij} = \left(R^h_{ij}\mathrm{C}_{ijkl} d^e_{kl} - R^h_{ij}\sigma_{ij} d^e_{kk}\right)k^h \quad [12]$$

By combining [12] and [10] and using the fact that plastic strain occurs with no volume change (without summation over h):

$$\dot{\gamma}^h + R^h_{ij}\sigma_{ij} d^e_{kk} k^h = R^h_{ij}\mathrm{C}_{ijkl}\left(d_{kl} - d^p_{kl}\right)k^h \quad [13]$$

From [13] one can deduce:

$$\left(\delta_{hg} + k^h R^h_{ij}\mathrm{C}_{ijkl} R^g_{kl}\right)\dot{\gamma}^g = \left(R^h_{ij}\mathrm{C}_{ijkl} d_{kl} - R^h_{ij}\sigma_{ij} d_{kk}\right)k^h \quad [14]$$

So the slip rate over the slip system g:

$$\dot{\gamma}^g = M_{gh} R'^h_{ij}\left(\mathrm{C}_{ijkl} - \sigma_{ij}\delta_{kl}\right)d_{kl} \quad [15]$$

Where:

$$M_{gh} = \left(\delta_{hg} + k^h R_{ij}^h C_{ijkl} R_{kl}^g\right)^{-1} \quad [16]$$

2.5. *Variables updating*

It is necessary to present the way to update all the problem variables. For the critical shear stress it is:

$$\dot{\tau}_c^g = H^{gh}\dot{\gamma}^h \quad [17]$$

The form of the hardening matrix H has been introduced by (Franciosi, 1984). This matrix has the mean dislocation density acting on each slip system as internal variable. The hardening matrix has been modified by further works and can be defined as (Tabourot, 1992; Berbenni, 2002; Paquin *et al.*, 2001):

$$H^{gh} = \frac{\alpha\mu}{2}\frac{a^{gh}}{\sqrt{a^{gk}\rho^k}}\left(\frac{1}{\bar{L}^h} - 2y_c\rho^h\right) \quad [18]$$

– α is a parameter calculated by minimising the free Gibbs' energy (Aubert, 1998) of a dislocation loop and can be calculated from the Poisson's ratio:

$$\alpha = \frac{\pi}{16}\frac{\upsilon - 2}{\upsilon - 1} \approx 0.48 \quad [19]$$

– b is the Burgers vector norm,

– μ is the shear modulus,

– ρ^h is the dislocation density on the system h,

– $\bar{L}^g$ is the mean free path of dislocation depending on a parameter g_0 and:

$$\bar{L}^g = g_0\left(\sqrt{\sum_{h\neq g}\rho^h}\right)^{-\frac{1}{2}} \quad [20]$$

In [18] there are 2 terms: the first one depending on the mean free path of dislocations and representing their creation and the second one, depending on the critical annihilation distance, representing their annihilation.

– y_c is the critical annihilation distance, which is linked to the initial critical resolved shear stress (Essmann *et al.*, 1979, Berbenni, 2002). in the case of two

screw dislocations of opposite sign which annihilate if the stress excess the stress required for dislocation glide the value of y_c is given by [21]

$$y_c = \frac{\mu b}{2\pi\tau_{c0}} \qquad [21]$$

[21] gives an idea of what can be the critical annihilation distance but not its exact value.

– a^{gh} is an interaction matrix depending on nine constants $(a_0..a_8)$ (Hoc, 1999). Each constant represent a type of interaction between two slip systems. The nine parameters of this matrix are assumed to be the same for each material studied in this paper. This matrix is completely defined in appendix.

The update of dislocation density has to be defined (Tabourot, 1992) without summation over g :

$$\dot{\rho}^g = \frac{1}{b}\left(\frac{1}{\bar{L}^g} - 2y_c\rho^g\right)\dot{\gamma}^g \qquad [22]$$

This formula is constructed on the same way than the hardening matrix.

The single crystal is oriented in the space by three Euler's angles (Hansen *et al.*, 1978). They are noted φ_1,ϕ,φ_2 and their evolution are only due to the rate of elastic rotation (Iwakuma *et al.*, 1983):

$$\dot{\varphi}_1 = -w_{12}^e - \frac{\cos\phi}{\sin\phi}\left(w_{13}^e\cos\varphi_1 + w_{23}^e\sin\varphi_1\right) \qquad [23a]$$

$$\dot{\phi} = -w_{23}^e\cos\varphi_1 + w_{13}^e\sin\varphi_1 \qquad [23b]$$

$$\dot{\varphi}_2 = -\frac{1}{\sin\phi}\left(w_{13}^e\cos\varphi_1 + w_{23}^e\sin\varphi_1\right) \qquad [23c]$$

2.6. *Elastic-Plastic constitutive law*

First the link between the nominal stress rate and Cauchy's one is given:

$$\dot{n}_{ij} = \hat{\sigma}_{ij} - w_{ik}^p\sigma_{kj} - w_{jk}^p\sigma_{ki} + \sigma_{ij}d_{kk} - d_{ik}\sigma_{kj} + w_{jk}\sigma_{ki} \qquad [24]$$

By combining with the elasticity law [11] and using the fact that trace of d^p is null, equation [24] gives:

$$\dot{\mathrm{n}}_{ij} = \left[\mathrm{C}_{ijkl} d_{kl} - d_{ik}\sigma_{kj} + w_{jk}\sigma_{ki}\right] + \left[-\mathrm{C}_{ijkl} d^{p}_{kl} - w^{p}_{ik}\sigma_{kj} - w^{p}_{jk}\sigma_{ki}\right] \quad [25]$$

By using [4], [15] and [25] and the symmetric properties of the elastic moduli tensor, one obtains:

$$\dot{\mathrm{n}}_{ij} = \left[\mathrm{C}_{ijkl} - \frac{1}{2}\left(\delta_{ik}\delta_{lm} + \delta_{il}\delta_{km}\right)\sigma_{mj} - \frac{1}{2}\left(\delta_{jk}\delta_{lm} - \delta_{jl}\delta_{km}\right)\sigma_{mi}\right] g_{lk} -$$
$$\left[\mathrm{C}_{ijkl} R^{g}_{kl} + S^{g}_{ik}\sigma_{kj} + S^{g}_{jk}\sigma_{ki}\right]\left[\delta_{hg} + R^{'h}_{ij}\mathrm{C}_{ijkl} R^{g}_{kl}\right]^{-1} k^{h} R^{h}_{ij}\left[\mathrm{C}_{ijkl} - \sigma_{ij}\delta_{kl}\right] g_{lk} \quad [26]$$

The expression of the elastic-plastic tangent modulus L finally is obtained:

$$\mathrm{L}_{ijkl} = \left[\mathrm{C}_{ijkl} - \frac{1}{2}\left(\delta_{ik}\delta_{lm} + \delta_{il}\delta_{km}\right)\sigma_{mj} - \frac{1}{2}\left(\delta_{jk}\delta_{lm} - \delta_{jl}\delta_{km}\right)\sigma_{mi}\right]$$
$$- \left[\mathrm{C}_{ijkl} R^{g}_{kl} + S^{g}_{ik}\sigma_{kj} + S^{g}_{jk}\sigma_{ki}\right]\left[\delta_{hg} + R^{'h}_{ij}\mathrm{C}_{ijkl} R^{g}_{kl}\right]^{-1} k^{h} R^{h}_{ij}\left[\mathrm{C}_{ijkl} - \sigma_{ij}\delta_{kl}\right] \quad [27]$$

Where:

$$\dot{n}_{ij} = L_{ijkl} g_{lk} \quad [28]$$

2.7. *Computational algorithm*

It is now interesting to present how the behavior law is implemented in a Fortran 77 code. Firstly, the integration scheme chosen is Euler's one for its simplicity. The major problem of such an explicit scheme is its dependence on the integration step. Because the first step is obligatory elastic it can lead to problems in elastic limit prediction. This is the case when authors want to simulate changing loading path (cf. page 17). But if the step size remains small Euler's method can give results without too large numerical errors. According to this, in the future, authors will make the integration thanks to the fourth order Runge-Kutta method more robust and reliable. A first attempt of this could be find in Lorrain *et al.* (2003).

The algorithm used can be put on the form:

1. Initialize the problem.

   – $\sigma = 0, L = C, \varepsilon = 0$

2. Read all initial parameters.

   $\tau_{c0}, y_c, g_0, \rho_0, a0...a8, E, \nu, \alpha, b$

3. Apply loading step.

   g

4. Calculate the Hardening matrix.

5. Determine active slip systems.

6. Calculate slip rate. Slip rates can be negative due to a matrix inversion in [15]. Is this case go to 4 by putting slip rate on those systems null.

7. Calculate internal variable increment.

$$\dot{\tau}_{c0}, \dot{\rho}, \dot{\varphi}_1, \dot{\phi}, \dot{\varphi}_2, \dot{\sigma}$$

8. Update stress and internal variables.

9. Go to next step.

In this approach, comparatively to more classical ones, all slip systems potentially active are assume active. No energy criterion is applied. In order to check validity of this model to other, comparative tests have been made from the paper of Nesterova *et al.* (2001). Those authors have simulate shear tests thanks to the full constraint Taylor model by assuming that slip occurs only on {1 1 1}<1 1 0> family. Results of the comparison are listed in table 2, with the slip systems numbering table 1.

Table 1. *Slip systems numbering for one family of slip systems*

Syst.	*n*	*m*	Syst.	*n*	*m*	Syst.	*n*	*m*
1	<111>	[1 $\bar{1}$ 0]	5	<$\bar{1}$11>	[101]	9	<1$\bar{1}$1>	[011]
2	<111>	[10$\bar{1}$]	6	<$\bar{1}$11>	[01$\bar{1}$]	10	<1$\bar{1}$1>	[1 $\bar{1}$ 0]
3	<111>	[01$\bar{1}$]	7	<1$\bar{1}$1>	[110]	11	<1$\bar{1}$1>	[101]
4	<$\bar{1}$11>	[110]	8	<1$\bar{1}$1>	[10$\bar{1}$]	12	<1$\bar{1}$1>	[011]

Table 2. *Comparison between active slip systems found by the present model and literature*

Rolling convention	Major slip system (Nesterova *et al.*,)	Minor slip system (Nesterova *et al.*,)	Major slip system (present model)	Minor slip system (present model)	Residual slip system
(111)[12$\bar{1}$]	8	2	8	2	1,4,6,7,9,10,12
(111)[1 $\bar{1}$ 0]	10	1	10	1	3,6,8,11,12
(111)[14$\bar{5}$]	10,8	1,2	10,8	1,2	3,5,6,7,12
(111)[$\bar{1}$51]	6,8	3,11	6,8	3	4,7,9
(001)[100]	2,3,5,6,8,9,11,12	None	2,3,5,6,8,9,11,12	None	None

Results Table 2 show that, in each case, the predicted major slip systems are the good ones, and in one case a minor one is not predicted by the model. But in the

present model other slip systems are also active. They are called residual ones because their slip rates are at least 100 times smaller than other slip systems ones. The new law for determining active slip systems is comparable to a elastic-viscoplastic one where all systems are active but only a few have a slip rate much larger than other (Paquin *et al.*, 2002). This allows to say that this new determination of active slip systems can be used instead of classical approaches.

3. Comparison between theory and experiment

Before introducing the behavior model in a scale transition scheme, it is necessary to validate this model by comparing numerical results with experimental ones. Experimental results are extracted from literature but crystalline orientation is never given by the authors: only two of the three Euler's angle are given. In these cases those parameters would be identified on one test and kept constant on the others. In each series of tests only τ_{c0}, y_c and g_0, which influence is independent from one to the others, have been identified from one figure:

– elastic limit allows to identify critical initial resolved shear stress,

– the beginning of the loading permits to identify the parameter linked to storage of dislocations,

– at larger strain the annihilation process has a strong influence, so it is possible to identify the critical annihilation distance.

Other parameters have classical value usually taken for polycrystalline steels. For the case of dislocation density, since no information about its value is given, it have been chosen a classical value for annealed steels. In order to obtain good results the identification procedure is made by taking as reference each test from literature, and only the best fit is presented here. Each direction test would be put in the standard triangle on every figure.

3.1. *Tensile tests*

The experimental tests are extracted from (Pollnow *et al.*, 1973), on seven specimens. The material used is an α-iron with a 0.001 weight % in carbon. Experimental difference between each test is the tensile direction. In order to validate the model, all parameters would be constant (except for the Euler's angles). Table 3 gives crystallographic orientation for each test. It has to be noted that the first Euler's angle is taken constant because two angles are sufficient to define a direction. Figures 2a to 2f are the model's validation.

– Figure 2a shows a good agreement between theory and experiment. Since elasticity is taken isotropic, the dependence of crystallographic initial orientation on the elastic limit is only taken into account thanks to crystalline plasticity. This is not sufficient to well predict the elastic limit of so elastically anisotropy single crystals.

In author's opinion it can explain the discrepancy between experimental and numerical results. It can also be seen that the hardening slope is rather the same between these two curves.

– Figure 2b shows a badly agreement than for 2a but the stress level is near the real one. The principal difference is that the hardening is not well calculated; this difference seems to be due that the critical initial resolved shear stress which is taken the same for each slip system family. Introducing a difference between those families have been experimentally already enlightened (Orlans-Joliet, 1989) and used by the authors to make a comparison to the work of Rauch (1992). Obtained results were better than the proposed here (Lorrain *et al.*, 2003).

– Figures 2c, 2d and 2e show a very good agreement between model and reality during the entire loading path. The single crystal orientation of these cases is different than the identifying one, this allows to validate the model.

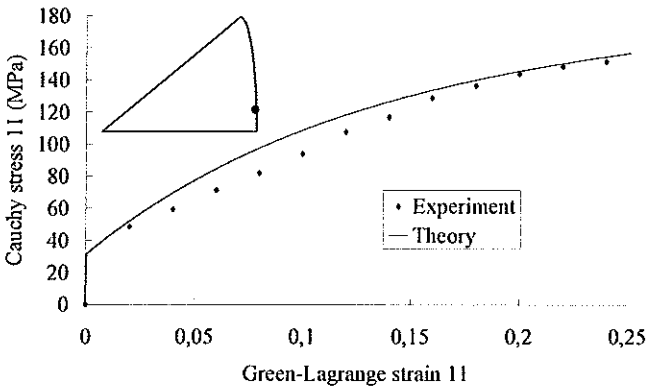

Figure 1. *Identifying curve for the tensile tests. Crystallographic orientation is 0°-82°-54°*

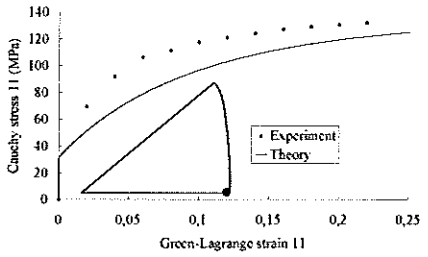

Figure 2a. *Validation for 0°-90°-45°*

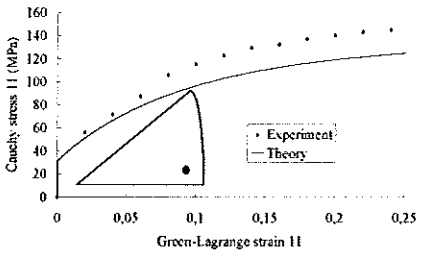

Figure 2b. *Validation for 0°-85°-45°*

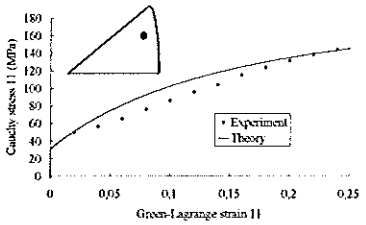

Figure 2c. *Validation for 0°-72°-55°*

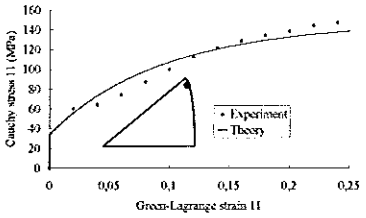

Figure 2d. *Validation for 0°-59°-45°*

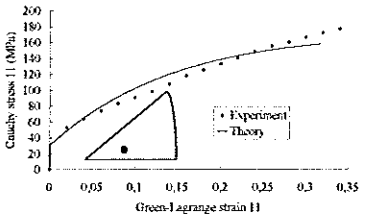

Figure 2e. *Validation for 0°-83°-62°*

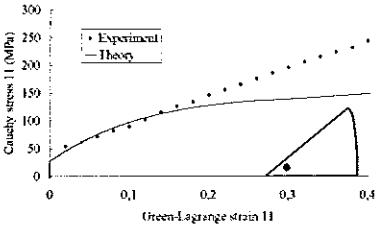

Figure 2f. *Validation for 0°-80°-74°*

Table 3. *Physical parameters for each set of tests*

Parameter	Tensile	Shear	Complex	Numerical
Young's Modulus E		$210000MPa$		
Poisson's ratio ν		0.3		
Bürgers vector norm b		$2.5.10^{-10}m$		
Parameter α		0.48		
Initial dislocation density ρ		$10^9 m^{-2}$		
Initial critical resolved shear stress τ_{c0}	$20MPa$	$20MPa$	$20MPa$	$100MPa$
Mean free path parameter g_0	220	220	370	10
Critical annihilation distance y_c	$4nm$	$2.7nm$	$0.9nm$	$5nm$

– Figures 2f shows a limitation of the model, the theoretical and experimental results are far from each other. An explanation is that the proposed model is not able to take into account so strong difference from one test to the other in terms of hardening slope. Especially if each family of slip systems have the same hardening

In a general way, the obtained results allow to say that the present model, with the assumptions of isotropic elasticity and the same initial critical resolved shear stress, is able to predict single crystal behavior which do not have a very strong elastic and plastic anisotropy.

3.2. *Simple shear tests*

The experimental tests are extracted from Keh *et al.*, 1967 on seven specimens. They have made shear test with different shear directions. The used material is an α-iron with a 0.0015 weight% in carbon. In order to validate the model the same procedure as in the previous part is adopted. Table 1 gives the identified parameters from figure 3. Table 4 gives crystallographic orientation for each test. It has to be noted that the first Euler's angle is taken constant because two angles are sufficient to define a direction. Figures 3a to 3f are the model's validation.

Table 4. *Crystallographic orientation for all numerical tests*

Figure	φ_1	ϕ	φ_2	Figure	φ_1	ϕ	φ_2
2	0°	82°	54°	4	0°	90°	45°
3a	0°	90°	45°	5a	0°	90°	0°
3b	0°	85°	45°	5b	0°	54°	45°
3c	0°	72°	55°	5c	0°	86°	45°
3d	0°	59°	45°	5d	0°	82°	45°
3e	0°	83°	62°	5e	0°	72°	45°
3f	0°	80°	74°	5f	0°	65°	45°
Figure	Path 1				Path 2		
	φ_1	ϕ	φ_2		φ_1'	ϕ'	φ_2'
6	60°	82°	66°		60°	82°	66°
7a	60°	82°	66°		60°	142°	10°
7b	60°	82°	66°		60°	52°	102°
7c	60°	82°	66°		60°	68°	80°
7d	60°	82°	66°		60°	102°	105°

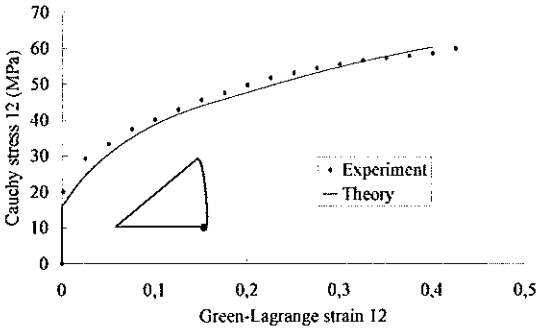

Figure 3. *Identifying curve for the simple shear tests. Crystallographic orientation is 0°-90°-45°*

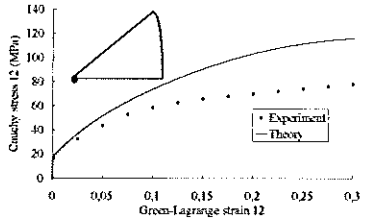

Figure 4a. *Validation for 0°-90°-0°*

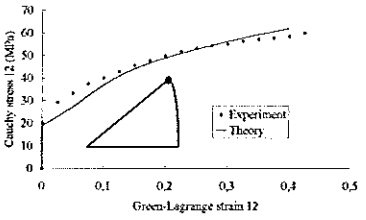

Figure 4b. *Validation for 0°-54°-45°*

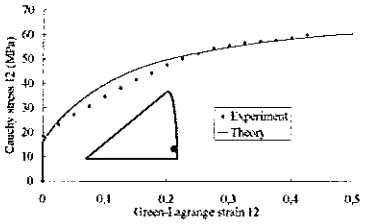

Figure 4c. *Validation for 0°-86°-45°*

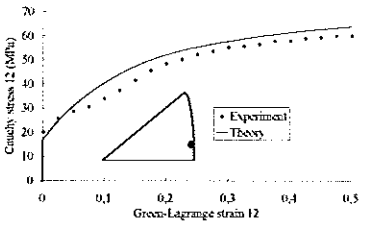

Figure 4d. *Validation for 0°-82°-45°*

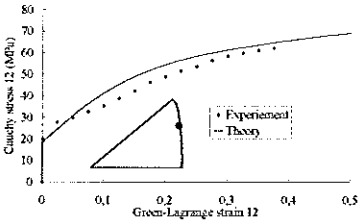

Figure 4e. *Validation for 0°-72°-45°*

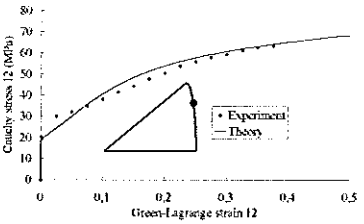

Figure 4f. *Validation for 0°-65°-45°*

– Figure 4a shows a result far from theoretical one. The hardening slope is very overestimated by compare to the real one. In this case the elastic limit is well estimated so the discrepancy, for the same reason as before, seems to be due to the initial critical resolved shear stresses.

– Figures 4b, 4c, 4d, 4e and 4f show very good agreement between theoretical and experimental tests during the entire loading path. The hardening slope is well taken into account, and the influence of initial critical shear stress (which is less marked than tensile tests) is also well calculated.

In a general way, the obtained results allow to say that the model is able to predict material behavior for shear tests. Results are better than for tensile test because the material does not show an anisotropy as strong as before which cannot been well reproduced because of authors' assumptions.

3.3. *Complex shear tests*

The experimental tests are extracted from Keh *et al.*, 1967 on five specimens. The tests are complex ones: a shear test followed by a shear test in another direction. The used material is the same as before but not at the same temperature; it explains why some parameters are different from the previous part. The experimental difference between each test is the second shear direction. In order to validate the model the same procedure as in the previous part is adopted. Table 3 gives the parameters identified from the figure 5. Table 4 gives crystallographic orientation for each test. Figures 6a to 6d are the model validation. In each figure the first path direction is represented by a rhomb and the second by a circle.

– Figure 6a shows a result far from theoretical one. The effect due to changing the loading path is very underestimated by compare with the real one. It can be explain by several facts: Firstly, for the same reasons as before concerning elastic limit and critical initial resolved shear stress. Secondly, when a changing of loading path occurs, dislocations microstructure created by the first path need to be broken in order to create a new one. This can have several effects, principally in a transitory stage at the second path beginning. Evidence of this can be found in Peeters, 2003.

– Figures 6b, 6c, and 6d show very good agreement between theoretical and experimental tests during the entire loading path. The effect of the loading path change is well reproduced by the model. But the same discrepancies at the beginning of the second loading can be also observed for the same reasons as figure 6a.

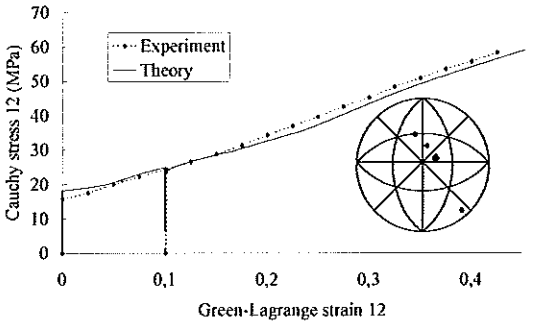

Figure 5. *Identifying curve for the complex shear tests. Crystallographic orientation is 60°-82°-66°/60°-82°-66°*

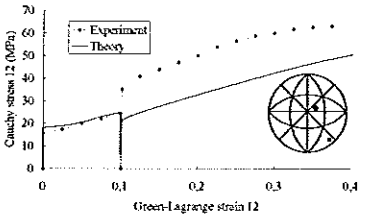

Figure 6a. *Orientation 60°-142°-10°*

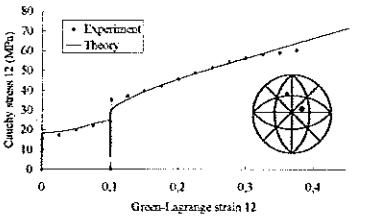

Figure 6b. *Orientation 60°-52°-102°*

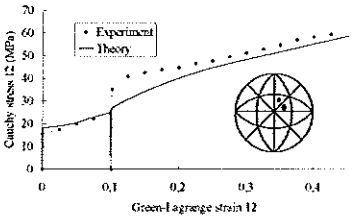

Figure 6c. *Orientation 60°-68°-80°*

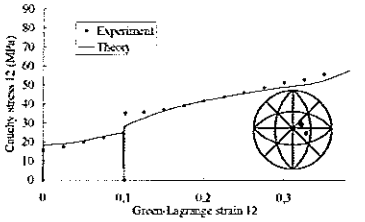

Figure 6d. *Orientation 60°-102°-105°*

In a general way, the obtained results allow to say that the model is able to predict material behavior for shear complex tests.

4. Ductility loss prediction

4.1. *Definition of the ductility loss criterion*

The aim of this part is to introduce a ductility loss criterion. Strain localization is bifurcation issued from a singularity (Petryk, 2000) at the level of the constitutive law defined by [28].

Many works to model this phenomenon have been made which consider that a localization condition is reached when there is ellipticity loss at the level of the solution (Asaro, 1983; Hill *et al.*, 1975; Peirce *et al.*, 1983). To describe this condition it is assumed that, during deformation, there is creation of a band on each part of whom there is not still continuity of fields. The formulation is extracted from the article of Rice (1976) but it can be seen in other forms (Asaro, 1983; Peirce, 1983; Peirce *et al.*, 1983; Petryk, 2000). Figure 7 shows this model.

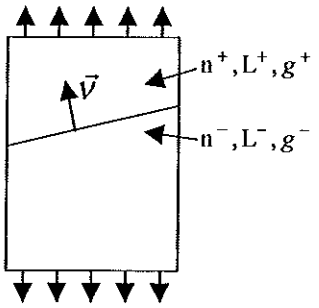

Figure 7. *Strain localization modelling*

The field equations have to be satisfied:

$$div\left(\dot{n}^T\right)=0 \qquad [29a]$$

$$g = grad(v) \qquad [29b]$$

$$\dot{n} = L : g \qquad [29c]$$

After the boundary conditions in term of stress or strain, depending on the simulated loading path, have to been added. It is assumed that no volume forces act on the system. Then the kinematics conditions of the strain rate jump is:

$$\left[g_{ij}\right]=g_{ij}^{+}-g_{ij}^{-}=\kappa_i v_j \qquad [30]$$

Where κ is the jump magnitude. Also it must have continuity of the normal forces along the interface created by the localization band:

$$\dot{n}_{ij}^{+}v_i=\dot{n}_{ij}^{-}v_i \Rightarrow \left[\dot{n}_{ij}\right]v_i=0 \qquad [31]$$

By using the behavior law [29c] in [30] one has:

$$L_{ijkl}^{+}g_{lk}^{+}v_i=L_{ijkl}^{-}g_{lk}^{-}v_i \qquad [32]$$

Which can be written on the form:

$$L_{ijkl}^{+}v_k v_i \kappa_l=\left(L_{ijkl}^{-}-L_{ijkl}^{+}\right)g_{lk}^{-}v_i \qquad [33]$$

When the localization band appears, it can be said that the tangent modulus is the same on each part of the band:

$$L^{+} = L^{-} = L \qquad [34]$$

By using the relation [34] in [29] one has:

$$L_{ijkl} v_i v_k \kappa_l = 0 \qquad [35]$$

From the equation [35], two classes of solutions can be extracted: either all the κ_l are zero then the magnitude of jumps is null; so there is no bifurcation in this case. Either at least one of the κ_l is not null and there is a system of equations which have an infinity of solutions from [35]:

$$\det\left(v_i L_{ijkl} v_k\right) = 0 \qquad [36]$$

4.2. *Qualitative results of the ductility loss criterion*

The aim of this part is to study the qualitative effect of physical parameters on the ductility loss. To do that, a reference test is made in which parameters (arbitrary chosen) are listed in Table 2. The crystallographic initial orientation is chosen thanks to the three Euler's angles by 0°,90°,0°.

The parameters which influence is studied are:

– critical initial resolved shear stress τ_{c0}

– mean free path parameter of dislocations g_0

– critical annihilation distance y_c

The different results obtained are shown figures 8 to 11. In the figures 8,10 and 11 are plotted the values of the minimum determinant value all over the space, normalized by the value for elasticity, versus the Green-Lagrange strain. The influence of those parameters would be seen through their capabilities for producing a lower/higher slope because the value of the determinant is related to the plastic one.

The figure 8 shows that the minimum determinant value decreases strongly at the beginning of the deformation and than increases until a local maximum; this corresponds to a "transitory regime" which is the onset of plasticity. After this maximum it can be seen that the curve is monotonically decreasing until reaching negative value. By reporting strain corresponding to $\det(vLv)$ equal to zero versus the initial critical resolved shear stress, figure 9, it can be seen that higher the elastic limit is, less the ductility is. This can be compared with the work of Luft, (1991) who has made molybdenum single crystal tensile tests with different temperatures. The deformation mechanisms and crystallographic structure of molybdenum are the

same than iron. Luft obtains roughly the same influence of the elastic limit than the one of the model. If it is assumed that in this test the change in elastic limit has a stronger influence than change in other physical parameters it validates the qualitative influence of initial critical resolved shear stress.

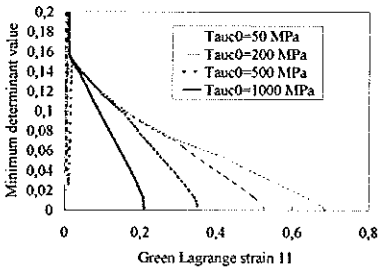

Figure 8. *Minimal normalized value of the determinant υLυ versus strain*

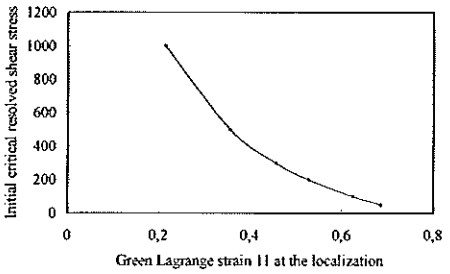

Figure 9. *Influence of the initial critical resolved shear stress on ductility loss*

In figures 10 and 11 are shown influence of two parameters of the hardening matrix [18], they have a dual influence because one is linked to storage and one to annihilation of dislocations. The figure 10 shows that the lower the mean free path of dislocations parameter is, the higher the ductility is; that is in agreement with reality because the lower this parameter is the more the storage of dislocation (so the consolidation) is. This argument is only valid for the case of mobile dislocation which are dominant in BCC single crystals. The figure 11 shows the dual effect of 10: the less the critical annihilation is the more the ductility is. This is also in agreement with reality: if the material does not annihilate dislocation it can store more and more dislocations so the ductility is increased. Those tests have also been made on other orientations not shown there for the sake of simplicity. But same results have been exhibited while changing crystallographic orientation.

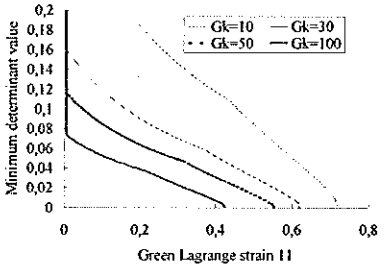

Figure 10. *Influence of the mean free path parameter on the ductility loss*

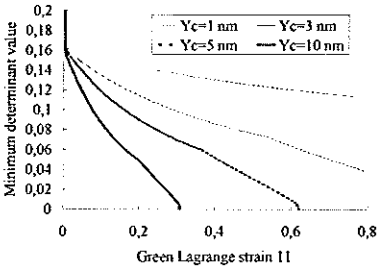

Figure 11. *Influence of the critical annihilation distance on the ductility loss*

5. Conclusions

In this work several results have been obtained:

– a single crystal elastic-plastic model in finite transformations framework is proposed. It is able to predict with a good accuracy the behavior of single crystal for simple and complex loading paths. Model parameters remain the same for one material and do not vary from a test to the others, which allows to validate the model,

– a ductility loss criterion has been introduced. It is able to qualitatively predict the effect of the parameters of the proposed model. These results are also qualitatively in good agreement with those of literature.

In the so saved room the proposed model seems to be good enough to be used in a scale transition scheme in order to simulate polycrystalline behavior and plot forming limit diagrams.

Acknowledgments

The authors wish to thank Xavier Lemoine and Mikhaël Balabane for scientific helpful discussions and Arcelor Research and Development for its financial support.

6. References

Asaro R. J., Rice J. R., "Strain localisation in ductile single crytals", *Journal of the Mechanics and Physics of Solids*, vol. 25, 1977, p. 309-338.

Asaro R. J., "Crystal plasticity", *Journal of Applied Mechanics*, vol. 50, 1983, p. 921-934.

Aubert I., Effet de l'hétérogénéisation plastique sur le comportement macroscopique lors de chargements complexes, Thèse, Université de Metz, 1998.

Ben Zineb T., Arbab Chirani S., Berveiller M., « Nouvelle formulation de la plasticité cristalline utilisant une contrainte de référence avec écrouissage », *15th Congress of Mechanics*, 3-7 septembre, 2001, Nancy.

Berbenni S., Elastoviscoplasticité des aciers polycristallins: modélisation micromécanique et physique Application au comportement dynamique et à l'effet Bake-Hardening, Thèse, Ecole Nationale Supérieure d'Arts et Métiers, 2002.

Berveiller M., Zaoui A., "An extension of the self-consistent scheme to plastically flowing polycristals", *Journal of the Mechanics and Physics of Solids*, vol. 26, 1979, p. 325-344.

Busso E.P., Cailletaud G., "On the numerical implementation of non-smooth domains, Part I: Rate dependent formulation" *Submitted for publication to the Journal de Physique*, 2002.

Essmann U., Mughrabi H., "Annihilation of dislocations during tensile and cyclic deformations and limits of dislocation densities", *Philosophical Magazine A*, vol. 40 n° 6, 1979, p. 731-756.

Franciosi P., Etude théorique et expérimentale du comportement élastoplastique de monocristaux métalliques se déformant par glissement: Modélisation pour un chargement complexe quasi statique, Thèse, Université Paris-Nord, 1984.

Franciosi P., Zaoui A., "Crystal hardening and the issue of uniqueness", *International Journal of Plasticity*, vol. 7, 1991, p. 295-311.

Hansen J., Pospiech J., Lücke K., *Tables for Texture Analysis of Cubic Crystals*, Berlin, Springer-Verlag, 1978.

Hoc T., Étude expérimentale de la localisation de la déformation plastique dans les aciers IF au cours de changement de trajet de déformation, Intermediary Report, Ecole Centrale Paris, 1998.

Hoc T., Etudes expérimentale et numérique de la localisation de la déformation lors de changements de trajets dans un acier doux, Thèse, Ecole Centrale Paris, 1999.

Hill R., Hutchinson J. W., "Bifurcation phenomena in the plane tension test", *Journal of the Mechanics and Physics of Solids*, vol. 23, 1975, p. 239-264.

Iwakuma T., Nemat-Nasser S., Finite elastic plastic deformation of polycrystalline metals and composites, Earthquake research laboratory technical Report No. 83-3-51, March 1983.

Keh A.S., Nakada Y., "Plasticity of iron single crystal", *Canadian Journal of Physics*, vol. 45, 1967, p. 1101-1120.

Kröner A., "Bounds for effective elastic moduli of disordered material", *Journal of the Mechanics and Physics of Solids*, vol. 25, 1977, p. 137-155.

Luft A., "Microstructural processes of plastic instabilities in strengthened metals" *Progress in material science*, vol. 35, 1991, p. 97-204.

Lorrain J. P., Ben Zineb T., Abed Meraim F., Berveiller M., « Modélisation du comportement élastoplastique de monocristaux de structure cubique, Comparaison théorie/expérience », *Proceedings of the 4th Journées Scientifiques et Techniques en Mécanique et Matériau*, 25-26 octobre 2002, Monastir Tunisia, p. 8-16.

Lorrain J. P., Ben Zineb T., Abed Meraim F., Berveiller M., Lemoine X., « Modélisation de l'influence des caractéristiques mécaniques sur la ductilité des matériaux cristallins », *Proceedings of 16th internatonal congress of mechanics*, Nice, 1-5septembre, 2003.

Mori T., Tanaka K., "Average stress in matrix and average elastic energy of materials with misfitting inclusions", *Acta Metallurgica*, vol. 21, 1973, p. 571-574.

Nesterova E. V., Bacroix B., Teodosiu C., "Microstructure and Texture Evolution under Strain Path Changes in Low-Carbon Interstitial-Free Steel", *Metallurgical and Material Transactions A*, vol. 32A, 2001, p. 2001-2527.

Orlans-Joliet B., Déformation plastique de monocristaux de structure cubique centrée en compression plane, Thèse, Ecole Nationale des Mines de Paris et Ecole Nationale Supérieure des Mines de Saint Etienne, 1989.

Paquin A., Berbenni, S., Favier V., Lemoine, X., Berveiller M. "Micromechanical modelling of the elastic-viscoplastic behavior of polycrystalline steels", *International Journal of Plasticity*, vol. 17, No. 9, 2001, p. 1267-1302.

Peeters B., Multiscale modelling of the induced plastic anisotropy in if steel during sheet foration, Thesis of Katholieke Universiteit, Leuven, 2002.

Peirce D., "Shear band bifurcation in ductile single crystals", *Journal of the Mechanics and Physics of Solids*, vol. 31, No. 2, 1983, p. 133-153.

Peirce D., Asaro R. J., Needleman A., "Material rate dependence and localized deformation in crystalline solids", *Acta Metallurgica*, vol. 31, No. 12, 1983, p. 1951-1976.

Petryk H., "General condition for uniqueness in material with multiple mechanisms of inelastic deformation", *Journal of the Mechanics and Physics of Solids*, vol. 48, 2000, p. 367-396.

Pollnow D., Penelle R., Lacombe D., "Etude de propriétés mécaniques et du taux de consolidation de monocristaux de fer déformés par traction à température ambiante", *Mémoires scientifiques revue métallurgique*, vol. LXX, No. 10, 1973, p. 703-714.

Rauch E. F. "Plastic anisotropy of sheet metals determined by simple shear tests", *Materials Science and Engineering*, vol. A241, 1998, p. 179-183.

Rice J. R., "The localisation of plastic deformation", *Proceedings of the 14th International Congress of Theoretical and Applied Mechanics*, 1976, p. 207-220.

Sidoroff F., Cours sur les grandes déformations, Ecole d'été de Sophia Antipolis, Report greco No. 51/1982, 8-10 septembre 1982.

Tabourot L., Loi de comportement élastoviscoplastique du monocristal en grandes transformations, Thèse, Université de Grenoble, 1992.

7. Appendix Interaction matrix

The interaction matrix introduced in the hardening matrix needs to be completely defined. Firstly numbering of slip systems is given in table A1.

Then the interaction matrix is given in Table A2 and value of parameters in Table A3. As can be seen in table A1 and table A2, this interaction matrix is made of 9 parameters. Each parameter define the interaction type between two slip systems. According to Hoc (1998) for BCC crystals two families of systems can be defined: the first family regrouping the easy slip system and the second difficult ones. Then depending on the interaction type considered (between two system of one family coplanar or not, or one of first family with one of the other coplanar or not) it allows to define nine interaction coefficient. The value of those coefficient have been obtained thanks to experimental tests (Hoc, 1999) on IF-steels and their value are simply reported here.

Table A1. *Slip systems numbering for two families*

Syst.	*n*	*m*	Syst.	*n*	*m*	Syst.	*n*	*m*
1	<111>	[1$\bar{1}$0]	9	<$\bar{1}$11>	[01$\bar{1}$]	17	<1$\bar{1}$1>	[121]
2	<111>	[10$\bar{1}$]	10	<$\bar{1}$11>	[1$\bar{1}$2]	18	<1$\bar{1}$1>	[21$\bar{1}$]
3	<111>	[01$\bar{1}$]	11	<$\bar{1}$11>	[12$\bar{1}$]	19	<1$\bar{1}$1>	[1$\bar{1}$0]
4	<111>	[1$\bar{1}$2]	12	<$\bar{1}$11>	[211]	20	<1$\bar{1}$1>	[101]
5	<111>	[1$\bar{2}$1]	13	<1$\bar{1}$1>	[110]	21	<1$\bar{1}$1>	[011]
6	<111>	[$\bar{2}$11]	14	<1$\bar{1}$1>	[10$\bar{1}$]	22	<1$\bar{1}$1>	[112]
7	<$\bar{1}$11>	[110]	15	<11$\bar{1}$>	[011]	23	<11$\bar{1}$>	[$\bar{1}$12]
8	<$\bar{1}$11>	[101]	16	<11$\bar{1}$>	[$\bar{1}$12]	24	<11$\bar{1}$>	[2$\bar{1}$1]

Table A2. *Coefficient of the inter-action matrix*

	1	2	3	4	5	6	7	8	9	10	11	12	13	14	15	16	17	18	19	20	21	22	23	24
1	a0	a1	a1	a4	a4	a4	a3	a3	a3	a5	a5	a5	a3	a3	a3	a5	a5	a5	a2	a3	a3	a5	a5	a5
2	a1	a0	a1	a4	a4	a4	a3	a3	a3	a5	a5	a5	a3	a2	a3	a5	a5	a5	a3	a3	a3	a5	a5	a5
3	a1	a1	a0	a4	a4	a4	a3	a3	a2	a5	a5	a5	a3	a3	a3	a5	a5	a5	a3	a3	a3	a5	a5	a5
4	a4	a4	a4	a6	a7	a7	a5	a5	a5	a8	a8	a8	a5	a5	a5	a8	a8	a8	a5	a5	a5	a8	a8	a8
5	a4	a4	a4	a7	a6	a7	a5	a5	a5	a8	a8	a8	a5	a5	a5	a8	a8	a8	a5	a5	a5	a8	a8	a8
6	a4	a4	a4	a7	a7	a6	a5	a5	a5	a8	a8	a8	a5	a5	a5	a8	a8	a8	a5	a5	a5	a8	a8	a8
7	a3	a3	a3	a5	a5	a5	a0	a1	a1	a4	a4	a4	a2	a3	a3	a5	a5	a5	a3	a3	a3	a5	a5	a5
8	a3	a3	a3	a5	a5	a5	a1	a0	a1	a4	a4	a4	a3	a3	a3	a5	a5	a5	a3	a2	a3	a5	a5	a5
9	a3	a3	a2	a5	a5	a5	a1	a1	a0	a4	a4	a4	a3	a3	a3	a5	a5	a5	a3	a3	a3	a5	a5	a5
10	a5	a5	a5	a8	a8	a8	a4	a4	a4	a6	a7	a7	a5	a5	a5	a8	a8	a8	a5	a5	a5	a8	a8	a8
11	a5	a5	a5	a8	a8	a8	a4	a4	a4	a7	a6	a7	a5	a5	a5	a8	a8	a8	a5	a5	a5	a8	a8	a8
12	a5	a5	a5	a8	a8	a8	a4	a4	a4	a7	a7	a6	a5	a5	a5	a8	a8	a8	a5	a5	a5	a8	a8	a8
13	a3	a3	a3	a5	a5	a5	a2	a3	a3	a5	a5	a5	a0	a1	a1	a4	a4	a4	a3	a3	a3	a5	a5	a5
14	a3	a2	a3	a5	a5	a5	a3	a3	a3	a5	a5	a5	a1	a0	a1	a4	a4	a4	a3	a3	a3	a5	a5	a5
15	a3	a3	a3	a5	a5	a5	a3	a3	a3	a5	a5	a5	a1	a1	a0	a4	a4	a4	a3	a3	a2	a5	a5	a5
16	a5	a5	a5	a8	a8	a8	a5	a5	a5	a8	a8	a8	a4	a4	a4	a6	a7	a7	a5	a5	a5	a8	a8	a8
17	a5	a5	a5	a8	a8	a8	a5	a5	a5	a8	a8	a8	a4	a4	a4	a7	a6	a7	a5	a5	a5	a8	a8	a8
18	a5	a5	a5	a8	a8	a8	a5	a5	a5	a8	a8	a8	a4	a4	a4	a7	a7	a6	a5	a5	a5	a8	a8	a8
19	a2	a3	a3	a5	a5	a5	a3	a3	a3	a5	a5	a5	a3	a3	a3	a5	a5	a5	a0	a1	a1	a4	a4	a4
20	a3	a3	a3	a5	a5	a5	a3	a2	a3	a5	a5	a5	a3	a3	a3	a5	a5	a5	a1	a0	a1	a4	a4	a4
21	a3	a3	a3	a5	a5	a5	a3	a3	a3	a5	a5	a5	a3	a3	a2	a5	a5	a5	a1	a1	a0	a4	a4	a4
22	a5	a5	a5	a8	a8	a8	a5	a5	a5	a8	a8	a8	a5	a5	a5	a8	a8	a8	a4	a4	a4	a6	a7	a7
23	a5	a5	a5	a8	a8	a8	a5	a5	a5	a8	a8	a8	a5	a5	a5	a8	a8	a8	a4	a4	a4	a7	a6	a7
24	a5	a5	a5	a8	a8	a8	a5	a5	a5	a8	a8	a8	a5	a5	a5	a8	a8	a8	a4	a4	a4	a7	a7	a6

Table A3. *Value of the interaction matrix coefficients*

Parameter	a0	a1	a2	a3	aa4	a5	a6	a7	a8
Value	1	1	1.15	1.15	1.05	1.1025	1.3	1.3	1.a495